Pharmaceutical Research, Vol. 25, No. 12, December 2008 (© 2008)
DOI: 10.1007/s11095-008-9654-8

Research Paper

Microfabricated Particles for Engineered Drug Therapies: Elucidation into the Mechanisms of Cellular Internalization of PRINT Particles

Stephanie E. A. Gratton,[1] Mary E. Napier,[1] Patricia A. Ropp,[1] Shaomin Tian,[1] and Joseph M. DeSimone[1,2,3,4,5]

Received March 3, 2008; accepted June 4, 2008; published online July 1, 2008

Purpose. To investigate the cellular internalization pathways of shape- and size-specific particles as a function of zeta potential in different cell types.
Methods. A top-down particle fabrication technique called PRINT was utilized to fabricate monodisperse 1 μm cylindrical particles. Cellular internalization of these PRINT particles was monitored using confocal microscopy, flow cytometry, and transmission electron microscopy. The endocytic pathway used by 1 μm cationic PRINT particles was evaluated using different inhibitory strategies. Cytotoxicity assays were used to determine the toxicity of both cationic and anionic PRINT particles in multiple cell types.
Results. Particle internalization was confirmed using confocal microscopy, flow cytometry and transmission electron microscopy. The mechanism of internalization of positively charged PRINT particles was found to be predominantly clathrin-mediated endocytosis and macropinocytosis with very few particles utilizing a caveolae-mediated endocytic pathway. The exposed charge on the surface of the particles had a significant effect on the rate of endocytosis in all cell types tested, except for the macrophage cells. No significant cytotoxicity was observed for all PRINT particles used in the present study.
Conclusions. Cylindrical 1 μm PRINT particles were readily internalized into HeLa, NIH 3T3, OVCAR-3, MCF-7, and RAW 264.7 cells. Particles with a positive zeta potential exhibited an enhanced rate of endocytosis compared to negatively charged particles with identical sizes and shapes. It was found that PRINT particles with a positive zeta potential were endocytosed into HeLa cells using predominantely clathrin-mediated and macropinocytotic pathways.

KEY WORDS: cellular uptake; endocytosis; particles; PRINT; surface charge.

INTRODUCTION

The exploration and utilization of nanocarriers for the delivery of therapeutics *in vivo* has led to dramatic improvements in the efficacy of various therapies. Over the past few years, intense research and development of novel platforms has resulted in drug delivery vehicles such as polymeric nanoparticles, micelles, immunoconjugates, DNA-polymer conjugates, dendrimers and liposomes [1–18]. These different vehicles have opened new avenues in the development of site-specific targeted drug delivery [4–6,8–11,19,20]. Clinically, the success of these carriers has been limited by the lack of control over size, chemical composition, uniformity, cell targeting and ability to consistently load and release known amounts of cargo [14,21,22]. Additional challenges faced by liposomal and micellular structures include the fact that they are dynamic "assemblies" (they are not stable objects) and there is little control over size and shape, especially over time in the biological milieu [19,23,24]. In addition, there are many other naturally occurring lipidic membranes present *in vivo* which lead to fusion and membrane reorganization and therefore leakage of cargo. Moreover, it is difficult to dial in the amount of cargo that one can kinetically trap or encapsulate in liposomes and it is even more difficult to have a series of liposomal structures that can release the cargo at will in a controlled time frame. Indeed most liposomal systems do not allow one to systematically vary the percentage of the cargo that can be encapsulated. As a result, in order to study dose dependencies with liposomal systems, researchers are forced to accomplish such critical experiments by physically blending liposomes containing cargo with cargoless liposomes in order to vary the dose of drug at constant liposomal dosing. Controlling the composition, size, shape, functionality and stability both *in vitro* and *in vivo* of nanocarriers is critical to the design of a fully realized delivery vehicle.

Elucidating the mechanisms by which organic particles of controlled size, shape, site-specific surface chemistry, tunable particle matrix composition and tunable modulus undergo endocytosis is of great importance. Understanding the interdependent roles that size, shape and surface and matrix

[1] Department of Chemistry and Carolina Center of Cancer Nanotechnology Excellence, University of North Carolina at Chapel Hill, Chapel Hill, North Carolina 27599, USA.
[2] Department of Chemical Engineering, North Carolina State University, Raleigh, North Carolina 27695, USA.
[3] Lineberger Comprehensive Cancer Center, University of North Carolina at Chapel Hill, Chapel Hill, North Carolina 27599, USA.
[4] Department of Pharmacology, University of North Carolina at Chapel Hill, Chapel Hill, North Carolina 27599, USA.
[5] To whom correspondence should be addressed. (e-mail: desimone@unc.edu)

composition have is particularly important. Once mechanisms of internalization are established, it is then possible to use these findings to better engineer the intracellular release of specific cargos. This information, in combination with ongoing efforts to understand the biodistribution of shape controlled particles [25], will help to establish rules towards the rational design of nanocarriers for the effective *in vivo* delivery of various cargos, especially those cargos that need to be internalized into cells such as siRNA and antisense oligonucleotides. The major endocytic pathways used by cells, for example, clathrin-mediated, caveolae-mediated, or macropinocytosis play prominent roles in the uptake and intracellular trafficking of organic particles. This study utilizes polymer and organic chemistry, biochemistry, and cell biology to investigate these mechanisms using a novel particle fabrication method called PRINT™ (Particle Replication In Non-wetting Templates) [22,26]. PRINT takes advantage of the unique properties of elastomeric molds comprised of a low surface energy perfluoropolyether network, allowing for the production of monodisperse, shape-specific particles from an extensive array of organic precursors [22,25,26]. Here, we will explore the internalization mechanisms of non-targeted 1 μm cylindrical PRINT particles.

MATERIALS AND METHODS

Materials

Fluorocur™, the perfluoropolyether used as the molding material in the PRINT process, was purchased from Liquidia Technologies (Product 2M-140). Trimethylolpropane ethoxylate triacrylate (M_n=428 g/mol; Aldrich), was passed through a short plug of alumina prior to use to remove inhibitor. Poly(ethylene glycol) monomethyl ether monomethacrylate (M_n=1,000 g/mol; Polysciences), fluorescein-*o*-acrylate (Aldrich), 2-aminoethyl methacrylate hydrochloride (Aldrich) and 2,2-diethoxyacetophenone (Aldrich) were used as received without further purification. Polyethylene sheeting was purchased from American Plastics Company. Silicon templates used as masters were obtained from Benchmark Technologies. Solvents used in the fabrication and purification of PRINT particles (2-propanol, and acetone) were filtered before use through a 0.22 μm PTFE syringe filter. Borax buffer was obtained from Ricca Chemical Company. HeLa, NIH 3T3 and RAW 264.7 cell lines were obtained from ATCC. The Lineberger Cancer Center Tissue Culture Facility, at the University of North Carolina Chapel Hill supplied the MCF-7 and OVCAR-3 cell lines. All cell culture media (MEM, OptiMEM) were purchased from the Lineberger Cancer Center Tissue Culture Facility at the University of North Carolina at Chapel Hill. Invitrogen supplied the GlutaMAX-I. Cell Titer 96® AQueous One Solution Cell Proliferation Assay was purchased from Promega. The 1.5 G cover slips were obtained from MatTek Corporation, and DRAQ5 was purchased from Biostatus, Ltd.. Molecular Probes supplied the Alexa Fluor-555 labeled wheat germ agglutinin, and Polysciences supplied the Polybed 812 epoxy resin. Nocodazole was obtained from Sigma.

Preparation of PRINT Particles

The fabrication of patterned Fluorocur™ molds has been described elsewhere [25,26]. The particle composition used for the 1 μm particles was 67 wt% trimethylolpropane ethoxylate triacrylate (MW=428 g/mol), 20 wt % poly(ethylene glycol) monomethylether monomethacrylate (MW=1,000 g/mol), 10 wt % 2-aminoethyl methacrylate hydrochloride (AEM HCl), 2 wt % fluorescein-*o*-acrylate, and 1 wt % 2,2-diethoxyacetophenone (Fig. 1). The monomers were weighed out into a 50 ml Falcon tube, then diluted with 2-propanol so that the solution contained 10 wt% monomers. This solution was sprayed onto a perfluoropolyether mold using an air gun. The mold was given 10 min to allow for additional 2-propanol evaporation. A polyethylene sheet was placed on top of the mold, and peeled back at a rate of 10 cm/min. The mold was then placed in a UV curing chamber. The chamber was purged with nitrogen for 2 minutes, then exposed to UV irradiation (λ= 365 nm, power=20 mW/cm^2) for 2 min, thereby curing the particles.

Particles were harvested into a drop of ~5 ml of filtered acetone by sliding a glass slide across the surface of the mold. By gently applying pressure, the particles were removed from the mold and were collected into a 50 ml Falcon tube. The particles were spun down using a centrifuge (IEC CENTRA CL2 Centrifuge, Thermo Electron Corporation) for 10 min at 3200 rpm, and were then rinsed four times with fresh acetone, dried in a vacuum desiccator overnight, weighed, then redispersed in the appropriate amount of water to make a particle concentration of 10 mg/ml.

To prepare negatively charged particles, the positively charged particles described above were redispersed into 5 ml of Borax buffer (instead of water). Next, 1 ml of acetic anhydride was added to the particle dispersion for 4 h which was found to amidate primary amines on the surface of the PRINT particles [confirmed by zeta potential measurements

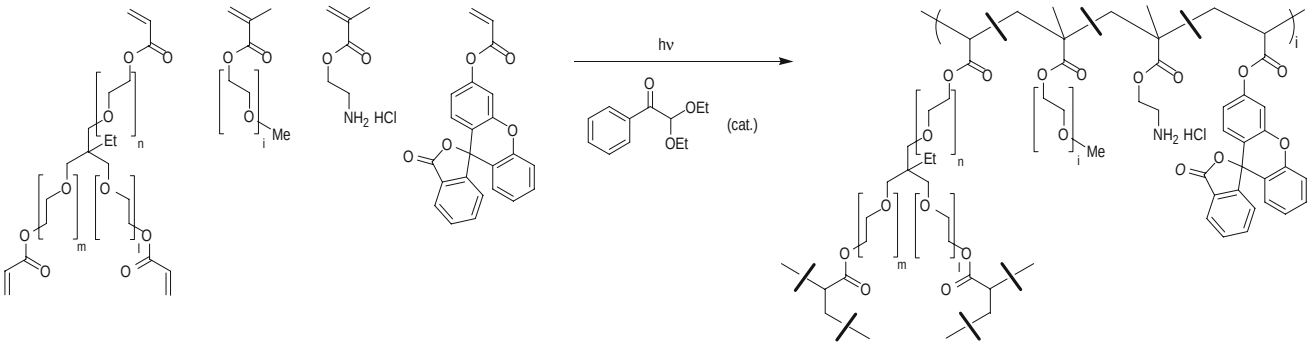

Fig. 1. Chemical structures of monomers and a partial structure of the PRINT particles.

(*vide infra*)]. Once the reaction was complete, 45 ml of acetone was added to the particle dispersion into a 50 ml Falcon tube, and the particles were spun down again, rinsed six times in fresh acetone, dried in a vacuum desiccator overnight, weighed, then redispersed in the appropriate amount of water to make a particle concentration of 10 mg/ml.

Particle Size Analysis of PRINT Particles using Scanning Electron Microscopy (in the dry state)

Scanning electron microscopy was used to measure the size of the PRINT particles using a Hitachi model S-4700 scanning electron microscope. Aqueous dispersions of particles were placed on a glass slide, the drop was then allowed to dry, and the glass slide was coated with 5.0 nm of Pd/Au alloy using a Cressington 108 auto sputter coater (Cressington Scientific Instruments Ltd.). Double-sided adhesive tape was used to adhere the Pd/Au coated glass slide to the sample holder. The sample was then placed inside the vacuum chamber of the SEM and observed under low vacuum (10^{-6} Torr).

Zeta Potential Measurements

The zeta potential of PRINT particles was measured using a ZetaPlus Zeta Potential Analyzer (Brookhaven Instruments Corporation). The average value was determined from an aqueous dispersion of PRINT particles at a concentration of 0.3 mg/ml and at a temperature of 25°C.

Cell Lines and Maintenance

HeLa cells were maintained in MEM supplemented with 10% FBS, 2 mM L-glutamine, 1 mM sodium pyruvate and non-essential amino acids. NIH 3T3 and RAW 264.7 cells were maintained in DMEM with 10% FBS, 4.5 g/l glucose, 2 mM L-glutamine, and 110 mg/l sodium pyruvate. MCF-7 cells were grown in RPMI 1640 with 10% FBS, 2 mM L-glutamine, 1 mM sodium pyruvate, non-essential amino acids, and 10 ug/ml insulin. OVCAR-3 cells were grown in RPMI 1640 supplemented with 10% FBS, 2 mM L-glutamine, 1 mM sodium pyruvate, 10 mM HEPES, 4.5 g/l glucose, and 10 μg/ml human recombinant insulin.

Cell Uptake and Cytotoxicity Assay

HeLa, MCF-7, OVCAR-3 and NIH 3T3 cells were seeded in 96 well plate at 2×10^4 per well, and RAW 264.7 cells were seeded at 5×10^4 per well. Cells were allowed to attach to the plate overnight at 37°C. The next day, 1 μm particles were vortexed and diluted in OPTI-MEM with GlutaMAX-I. Cells were briefly washed using OPTI-MEM with GlutaMAX-I and then dosed with particles for 4 h (50 μl/well). The particles were removed at the end of dosing. For uptake assays, cells were washed with DPBS and trypsinized. Cells were then treated with 0.1% trypan blue at room temperature for 10 min to quench the extracellular fluorescence from non-internalized particles [27]. Finally, cells were washed and resuspended in DPBS and analyzed on a Cyan flow cytometer (DakoCytomation) with Summit 4.3 software. For the cytotoxicity assays, 100 μl of complete growth medium was replaced in each well, and 20 μl of Cell Titer 96® AQueous One Solution Cell Proliferation Assay reagent was added and incubated at 37°C until color was well developed. The adsorptions at 490 nm were taken for analysis.

Confocal Laser Scanning Microscopy

HeLa cells (50,000) were seeded in a T-25 flask for 24 h (37°C, 5% CO_2). Following this, cells were washed one time with D-PBS followed by MEM with supplements containing 1% fetal bovine serum (low serum). Cells were then incubated for 4 h (37°C, 5% CO_2) with low serum MEM (2 ml) containing 15 μg/ml fluorescein-labeled PRINT particles. The cells were then detached with trypsin, resuspended in complete MEM containing 10% FBS, replated onto 2 35 mm^2 glass bottom dishes with 1.5 G cover slips and allowed to adhere over night at 37°C. Nuclei were stained with 2.5 μM DRAQ5 in complete MEM following the manufacturer's protocol. DRAQ5 is a DNA specific dye with far-red fluorescent properties (Ex: 647 nm, Em: 670 nm) [28]. Plasma membranes were visualized with AlexaFluor-555 labeled wheat germ agglutinin (WGA) in D-PBS (2.5 μg/ml). Cells were then fixed with 4% paraformaldehyde. An Olympus FV500 confocal laser scanning microscope (Olympus Co Ltd located in the Microscopy Laboratory Services, a core facility of the Department of Pathology and Laboratory Medicine) was used to visualize the cells. Z stacks were collected and used for 3-D reconstruction and visualization of intracellular uptake and particle localization within the cells.

Transmission Electron Microscopy (TEM)

Further evidence of particle internalization and translocation was gained using TEM. Here, 60 mm^2 polystyrene dishes were used to seed ~5×10^5 HeLa cells overnight. Cells were treated with PRINT particles the following day. Monolayers of cells were rinsed with D-PBS and fixed in 2% paraformaldehyde/2.5% glutaraldehyde/0.15 M sodium phosphate at pH 7.4, for several hours or overnight. Following three rinses with sodium phosphate buffer, the monolayers were post-fixed for 1 h in 1% osmium tetroxide/1.25% potassium ferrocyanide/0.15 M sodium phosphate buffer. After rinsing in deionized water, the cells were dehydrated using increasing concentrations of ethanol (30%, 50%, 75%, 100%, 100%, 10 min each) and embedded in Polybed 812 epoxy resin. A diamond knife was used to section the monolayers both parallel and perpendicular to the substrate. Ultrathin sections were collected on 200 mesh copper grids and stained with 4% aqueous uranyl acetate for 15 min, followed by Reynolds' lead citrate for 7 minutes. A LEO EM910 transmission electron microscope operating at 80 kV (LEO Electron Microscopy Inc. located at the Microscopy Laboratory Services Core Facility at UNC) was used to image the samples. Digital images were acquired using a Gatan Orius SC1000 CCD Digital Camera and Digital Micrograph 3.11.0 (Gatan, Inc.).

Microtubule Disruption

Nocodazole was used to determine the effect of disrupting microtubule depolymerization on the particle internalization. Cells were pre-incubated with 20 μM Nocodazole in serum-

free MEM for 60 min at 37°C/5% CO_2. The media was then removed and replaced with 20 μM Nocodazole in serum-free MEM containing 15 μg/ml 1 μm PRINT particles. Incubation at 37°C/5% CO_2 was continued for an additional 60 min and then processed by flow analysis.

Energy Dependent Uptake

Cells were pre-incubated in the presence of 0.1% NaN_3/50 mM 2-deoxyglucose (NaN_3/DOG) in serum-free MEM for 60 min at 37°C/5% CO_2 prior to incubation in the same media containing 15 μg/ml 1 μm particles. Cells were incubated with particles for 60 min at 37°C/5% CO_2 and then processed for analysis by flow cytometry.

Disruption of Clathrin-mediated Internalization

Cells were incubated in serum-free MEM containing 75 μM Dynasore for 60 min at 37°C/5% CO_2. Cells were subsequently incubated in serum-free MEM/75 μM Dynasore containing 15 μg/ml particles for 60 min and then processed for flow cytometry.

Cholesterol Depletion

Cells were pre-incubated with 2 μg/ml filipin (freshly prepared) in serum-free MEM for 60 min in 37°C/5% CO_2. The cells were then incubated in the same media containing 15 μg/ml particles for 60 min at 37°C/5% CO_2 and then subsequently processed analysis by flow cytometry.

RESULTS

Particle Characterization

The mean size and morphology of the PRINT particles were determined by SEM. The results show that the particles have a mean width of 1.00±0.06 μm, a mean height of 0.68±0.05 μm, with an apparent meniscus on one side of the particle (Fig. 2). The zeta potential of the positively charged particles was measured to be +23±3 mV using a ZetaPlus Zeta Potential Analyzer. Upon reaction of the surface amine groups with acetic anhydride for 4 h, the zeta potential changed from +23±3 mV to −19±3 mV.

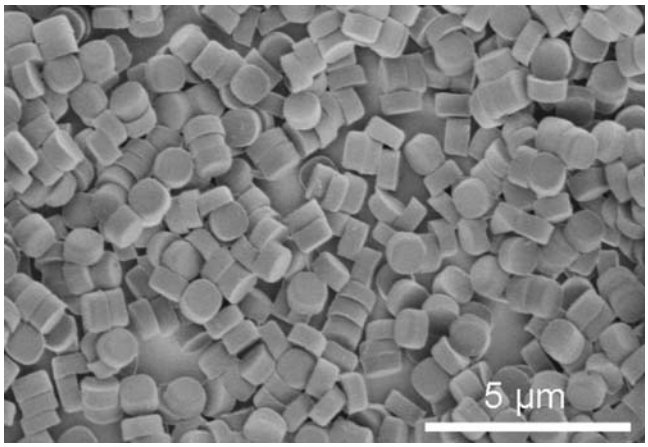

Fig. 2. A representative scanning electron micrograph of the 1 μm cylindrical particles used in the present study.

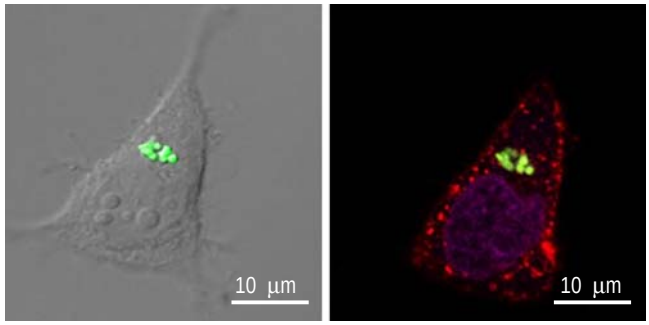

Fig. 3. Confocal micrographs of 1 μm PRINT particles internalized in HeLa cells after a 4 h incubation period.

Particle Internalization

Internalized particles were observed using multiple techniques including confocal microscopy, flow cytometry, and transmission electron microscopy (TEM). Figure 3 shows confocal micrographs of HeLa cells with internalized PRINT particles possessing a positive surface charge. In these experiments, cells were stained with AlexaFluor-555 labeled WGA to visualize the plasma membrane, and DRAQ5 to differentiate the cellular nucleus. Z stacks were collected and used for 3-D reconstruction and visualization of intracellular particle localization. Additionally, transmission electron micrographs were obtained to further demonstrate cellular internalization. Figure 4 shows 1 μm PRINT internalized particles in HeLa cells using TEM. It should be noted that multiple 1 μm PRINT particles can be internalized into a single cell.

Particle Internalization Pathways

Chemical inhibitors were used to assess the pathways used by HeLa cells to internalize 1 μm positively charged PRINT particles (Fig. 5). First, NaN_3/2-deoxyglucose (NaN_3/DOG) was exposed to the cells and a 70% decrease in internalization was observed signifying that the internalization pathways were energy dependent. The combination of NaN_3 and DOG impairs energy dependent translocation events by depleting ATP [29]. Filipin, a polyene antibiotic which sequesters plasma membrane cholesterol was used to investigate particle internalization by a caveloae-mediated mechanism. A ~2% decrease in internalization was seen when filipin was used to inhibit endocytosis. Dynasore, a cell permeable reversible inhibitor of dynamin was used to probe internalization via clathrin-coated pits [30]. Here, a 35% decrease in internalization of PRINT particles was seen. Finally, Nocodazole was used as an inhibitor of macropinocyotsis. Using Nocodazole, a 16% decrease in internalization was observed. These results suggest that multiple pathways are utilized for the internalization of PRINT particles into HeLa cells, with the predominant pathways being clathrin-mediated endocytosis, and macropinocytosis.

The Effect of Charge on Internalization

Flow cytometry was used as an additional *in vitro* technique to confirm cellular internalization. Here, positively and negatively charged PRINT particles were dosed onto HeLa (human epithelial carcinoma cells), NIH 3T3 (mouse

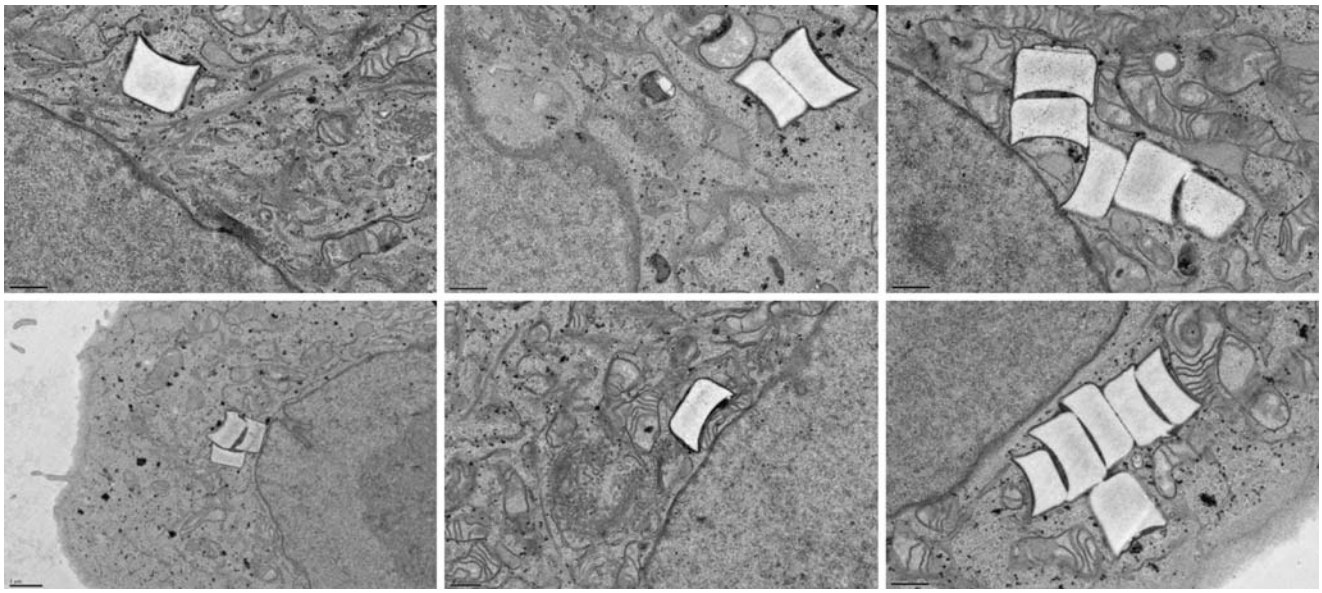

Fig. 4. Transmission electron micrographs of 1 μm PRINT particles internalized in HeLa cells after a 4 h incubation period.

embryonic fibroblast cells), OVCAR-3 (human ovarian carcinoma cells), MCF-7 (human breast adenocarcinoma cells), and RAW 264.7 (mouse leukaemic monocyte macrophage cells) for either 1 or 4 h of incubation (Fig. 6). Following several rinsing steps attempting to remove any membrane-bound or non-internalized particles, the percent of cells with internalized particles was measured on a Dako flow cytometer. With the exception of the macrophage cell line where there was no preferential internalization based on charge, all cells clearly show a preferential uptake of the positively charged particles over the negatively charged particles at all particle dosings tested (up to 360 μg/ml).

Specifically, it was found that at a particle concentration of 100 μg/ml, positively charged were internalized into ~100% of all the HeLa cells being analyzed, whereas only ~60% of the negatively charged particles were internalized at similar concentrations. When NIH 3T3 cells were investigated at the same particle concentration, a larger discrepancy was seen between the positively and negatively charged PRINT particles. Here, the positively charged particles were internalized by ~100% of the cells, while the negatively charged particles were only internalized by ~40% of the cells. In contrast, OVCAR-3 cells seemed to be less discriminatory, with ~100% of cells possessing an internalized positively charged particle, and ~80% of cells having an internalized negatively charged particle, both at particle concentrations of 100 μg/ml. An additional cancer cell line was examined, MCF-7 cells, which showed a more pronounced preference for the positively charged particles. In this case, at 100 μg/ml, ~80% of cells contained an internalized positively charged particle, whereas only ~40% of cells contained an internalized negatively charged particle. Finally, the macrophage cell line showed little, if any, effect of charge on particle internalization at all particle concentrations. For example, at 100 μg/ml ~85% of cells contained an internalized positively charged particle, and ~75% of cells contained an internalized negatively charged particle.

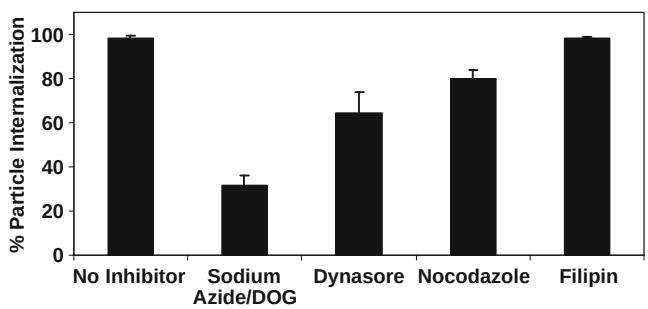

Fig. 5. Determining the cellular internalization pathway of 1 μm positively charged PRINT particles.

Cytotoxicity

The cytotoxicity of the PRINT particles used herein was evaluated using HeLa, NIH 3T3, OVCAR-3, MCF-7, and RAW 264.7 cells after 4 h of incubation with both positively and negatively charged 1 μm PRINT particles. In all five cell lines tested, no significant amount of cytotoxicity was observed (Fig. 6). Moreover, no observable cell death was seen for particles having either positive or negative zeta potentials. However, several cells lines showed a slight decrease in cell viability with an increase in particle concentration, while remaining relatively non-toxic. For example, HeLa cells show a ~12% decrease in cell viability once both positively and negatively charged particle concentrations were increased to 200 μg/ml and RAW 264.7 cells showed a decrease in cell viability (~13%) for both charged particles at concentrations of 125 μg/ml. For the remaining cell lines, i.e. NIH 3T3, OVCAR-3 and MCF-7, both surface charges showed no observable cell death at particle concentrations as high as 200 μg/ml. For all cell lines, cytotoxicity tests were performed with extended times (out to 72 h), with no significant amount of cell death observed (data not shown). It should be noted that all *in vitro* work performed in this study for confocal

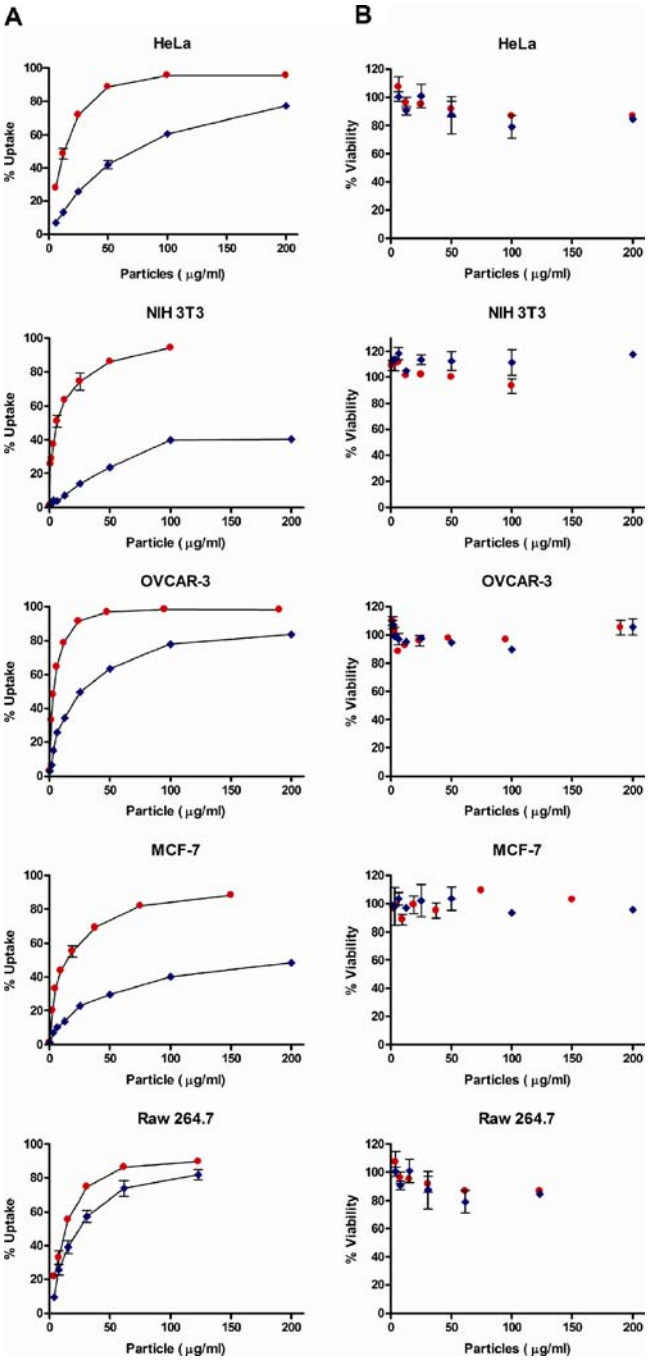

Fig. 6. Internalization of 1 μm PRINT particles by various cell lines. Cells were dosed with various concentrations of particles for 4 h at 37°C. **A** Cellular internalization profiles; **B** cytotoxicity of particles. *Red circles* represent positively charged particles; *blue circles* represent negatively charged particles. The data shown were representative of more than three separate experiments.

microscopy, inhibitory studies, and TEM were done at particle concentrations of 15 μg/ml, where no cytotoxicity was observed for any of the cell lines examined.

DISCUSSION

Major strides towards improving current particle delivery technologies will be possible once an understanding of the fate of particles *in vitro* and *in vivo* is clearly understood. Heretofore, this knowledge was difficult to ascertain due to the lack of "calibration quality" particles, where size, shape and surface chemistry is controlled and identical across all particles in a given lot of particles. PRINT technology allows for the fabrication of "calibration quality" particles with complete control over size, shape, and surface chemistry. In these studies, 1 μm cylindrical particles were chosen to facilitate microscopy studies where the visualization of individual internalized particles was possible. The size and shape of the cylindrical particles was examined using SEM (Fig. 2). The cylindrical particles display a meniscus on one side of the particles, which is a direct result of the PRINT process where capillary action is used to fill the perfluoropolyether molds. Once the liquid in the PRINT molds is polymerized, the meniscus becomes a permanent part of the particle shape.

Particle internalization was monitored using confocal microscopy, transmission electron microscopy (TEM), and flow cytometry. Figure 3 shows internalized 1 μm positively charged PRINT particles into HeLa cells by confocal microscopy. In these experiments both the plasma membrane and the nuclear membrane were stained to aid in differentiating membrane-bound particles from those that were internalized. Z stacks were collected and used for 3-D reconstruction of the internalized particles to further show internalized particles and intracellular location. TEM micrographs clearly show internalized 1 μm positively charged PRINT particles into HeLa cells, and the translocation of these particles (Fig. 4). Both confocal microscopy and TEM show the translocation of the positively charged PRINT particles to the perinuclear region of the cell, where, within a 60 minute incubation period, the majority of the internalized particles are localized at the perinuclear region of the cells. It should be noted that it is possible for more than one particle to be internalized into a single cell, as seen by both confocal microscopy and TEM.

In order to further understand the fate of particles once internalized, a series of inhibitors were used to examine the endocytic pathways used by positively charge PRINT particles (Fig. 5). Based on the results obtained, all particle internalization occurs via an energy dependent process as seen by the drastic decrease in internalization once NaN_3/DOG is applied to the cells (~70% decrease). NaN_3/DOG is known to block ATP synthesis and to impair energy dependent translocation. It is thought that complete inhibition was not accomplished due to exogenous ATP and glucose which are present in the serum-free media. Dynasore was used to inhibit clathrin-coated pit pathways by acting as a Dynamin GTPase inhibitor, and a ~35% decrease was observed in particle internalization with this inhibitory process. A ~16% decrease in internalization was observed when the macropinocytosis pathways were inhibited by inhibiting the microtubule depolymerization using Nocodazole. In contrast, only a ~2% decrease in internalization was seen when a caveolae inhibitor, filipin was used. Filipin is a polyene antibiotic which is known to bind cholesterol in the plasma membrane and inhibit caveolae-mediated endocytosis. It should be noted that additional modes of endocytosis exist such as non-clathrin, non-caveolae mediated endocytosis, which were not screened in the inhibition studies and could account for supplementary pathways of internalization utilized by these cationic 1 μm PRINT particles. Based on these results, it can be said that 1 μm positively charged cylindrical PRINT particles are

internalized using multiple pathways into the cell, and that internalization occurs predominantly by a clathrin-mediated endocytic pathway as well as macropinocytosis and not via caveolae-mediated endocytosis to any significant amount.

The effect that charge has on cellular internalization pathways has been studied [31]. It has been shown that positively charged D,L-poly(lactide) particles are internalized into HeLa cells using clathrin-mediated pathways whereas negatively charged D,L-poly(lactide) particles do not utilize the clathrin-mediated endocytotic pathway. Despite this study, little is known about the mechanism of the endocytotic machinery involved with internalized non-spherical particles, especially as a function of size, as well as the intracellular trafficking that takes place with non-spherical particles. To determine the effect of charge on different types of cells, negatively charged particles were also synthesized. Treating the surface amine groups of the positively charged particles with acetic anhydride in Borax buffer changed the zeta potential from +23±3 mV to −19±3 mV. Here, the negatively charged particles have retained the exact shape of the positively charged particles used in these studies, which showcases the ease of transformations of the surface chemistry on PRINT particles. In order to determine the effect of charge in multiple different cell lines, HeLa (human epithelial carcinoma), NIH 3T3 (mouse embryonic fibroblast), OVCAR-3 (human ovarian carcinoma), MCF-7 (human breast adenocarcinoma), and RAW 264.7 (mouse leukaemic monocyte macrophage) cells were used. In these experiments, HeLa, NIH 3T3, OVCAR-3, and MCF-7 cells all displayed a decreased rate of endocytosis with the negatively charged particles when compared to the identically sized and shaped positively charged particles at all particle concentrations tested (Fig. 6). In contrast, the RAW 264.7 macrophage cells showed no preferential uptake of positively charged particles over the negatively charged particles. In this series of experiments, both 1 and 4 h particle incubation times were examined, with little difference in cellular internalization observed with increased incubation times. These results suggest that a targeted particle therapy could be achieved at the appropriate particle dosing levels (~15 μg/ml) using negatively charged particles with a targeting ligand thereby avoiding non-specific uptake and increasing targeting efficiencies into the desired cells.

Since it is known that positively charged particles can induce cytotoxic effects, all particles used in this study were examined for cytotoxicity. It is thought that positively charged particles can disrupt the cellular membrane through electrostatic interactions with the cell membrane phospholipids [32,33]. In all cell lines tested, no significant cytotoxicity was observed after a 4 h incubation period with the cells (Fig. 6). The cytotoxicity assays were taken out to 72 h with no significant observable cell death.

CONCLUSION

A complete understanding of the molecular mechanisms involved for the internalization of particles into cells, as well as their fate once internalized, is crucial to the development of successful particle therapies. Here, we describe some initial studies investigating the endocytic pathways involved in particle internalization, as well as the effects of internalization based on particles having identical sizes, and shapes, but different surface chemistry, where one has a positive zeta potential and the other had a negative zeta potential. A pronounced preference for positively charged particles was seen in all cell lines except for the macrophage cells. Cytotoxicity was performed on all cell lines using both positively and negatively charged particles with no significant toxicity observed at all particle concentrations tested. Obtaining knowledge on the endocytic pathway used from "calibration quality" particles should lead to crucial information required for not only enhancing specific cellular internalization, but also manipulating the intracellular location of particles, and minimizing cytotoxic effects.

ACKNOWLEDGEMENTS

This work was supported in part by the STC Program of the NSF (CHE-9876674), NIH PPG P01-GM059299-07, NIH 5-654-CA119343-02 (the Carolina Center of Cancer Nanotechnology Excellence), the William R. Kenan Professorship of the University of North Carolina at Chapel Hill, and Liquidia Technologies (SRA 04-0013).

REFERENCES

1. A. D'Emanueleand, and D. Attwood. Dendrimer-drug interactions. *Adv. Drug Deliv. Rev.* **57**:2147–2162 (2005) doi:10.1016/j.addr.2005.09.012.
2. N. C. Bellocq, D. W. Kang, X. H. Wang, G. S. Jensen, S. H. Pun, T. Schluep, M. L. Zepeda, and M. E. Davis. Synthetic biocompatible cyclodextrin-based constructs for local gene delivery to improve cutaneous wound healing. *Bioconjug. Chem.* **15**:1201–1211 (2004) doi:10.1021/bc0498119.
3. M. A. Wolfert, P. R. Dash, O. Nazarova, D. Oupicky, L. W. Seymour, S. Smart, J. Strohalm, and K. Ulbrich. Polyelectrolyte vectors for gene delivery: Influence of cationic polymer on biophysical properties of complexes formed with DNA. *Bioconjug. Chem.* **10**:993–1004 (1999) doi:10.1021/bc990025r.
4. S. M. Moghimi, A. C. Hunter, and J. C. Murray. Nanomedicine: current status and future prospects. *FASEB J.* **19**:311–330 (2005) doi:10.1096/fj.04-2747rev.
5. Y. Barenholz. Liposome application: problems and prospects. *Curr. Opin. Colloid Interface Sci.* **6**:66–77 (2001) doi:10.1016/S1359-0294(00)00090-X.
6. R. Duncan. The dawning era of polymer therapeutics. *Nature Reviews Drug Discovery.* **2**:347–360 (2003) doi:10.1038/nrd1088.
7. G. S. Kwonand, and K. Kataoka. Block-Copolymer Micelles as Long-Circulating Drug Vehicles. *Adv. Drug Deliv. Rev.* **16**:295–309 (1995) doi:10.1016/0169-409X(95)00031-2.
8. C. C. Lee, J. A. MacKay, J. M. J. Frechet, and F. C. Szoka. Designing dendrimers for biological applications. *Nat. Biotechnol.* **23**:1517–1526 (2005) doi:10.1038/nbt1171.
9. K. McAllister, P. Sazani, M. Adam, M. J. Cho, M. Rubinstein, R. J. Samulski, and J. M. DeSimone. Polymeric nanogels produced via inverse microemulsion polymerization as potential gene and antisense delivery agents. *J. Am. Chem. Soc.* **124**:15198–15207 (2002) doi:10.1021/ja027759q.
10. V. P. Torchilin. Targeted polymeric micelles for delivery of poorly soluble drugs. *Cell. Mol. Life Sci.* **61**:2549–2559 (2004) doi:10.1007/s00018-004-4153-5.
11. M. J. Vicentand, and R. Duncan. Polymer conjugates: nanosized medicines for treating cancer. *Trends Biotech.* **24**:39–47 (2006) doi:10.1016/j.tibtech.2005.11.006.
12. H. P. Zobel, F. Stieneker, S. A. A. Aziz, M. Gilbert, D. Werner, C. R. Noe, J. Kreuter, and A. Zimmer. Evaluation of aminoalkylmethacrylate nanoparticles as colloidal drug carrier systems. Part II: characterization of antisense oligonucleotides loaded

copolymer nanoparticles. *Eur. J. Pharm. Biopharm*. **48**:1–12 (1999) doi:10.1016/S0939-6411(99)00003-X.
13. H. P. Zobel, A. Zimmer, S. A. A. Aziz, M. Gilbert, D. Werner, C. R. Noe, J. Kreuter, and F. Stieneker. Evaluation of aminoalkylmethacrylate nanoparticles as colloidal drug carrier systems. Part I: synthesis of monomers, dependence of the physical properties on the polymerization methods. *Eur. J. Pharm. Biopharm*. **47**:203–213 (1999) doi:10.1016/S0939-6411(98)00100-3.
14. R. Langer. Drug delivery and targeting. *Nature*. **392**:5–10 (1998).
15. R. P. Kulkarni, D. D. Wu, M. E. Davis, and S. E. Fraser. Quantitating intracellular transport of polyplexes by spatio-temporal image correlation spectroscopy. *Proc. Natl. Acad. Sci. U. S. A*. **102**:7523–7528 (2005) doi:10.1073/pnas.0501950102.
16. N. C. Bellocq, S. H. Pun, G. S. Jensen, and M. E. Davis. Transferrin-containing, cyclodextrin polymer-based particles for tumor-targeted gene delivery. *Bioconjug. Chem*. **14**:1122–1132 (2003) doi:10.1021/bc034125f.
17. S. Svensonand, and D. A. Tomalia. Commentary - Dendrimers in biomedical applications - reflections on the field. *Adv. Drug Deliv. Rev*. **57**:2106–2129 (2005) doi:10.1016/j.addr.2005.09.018.
18. R. Duncanand, and L. Izzo. Dendrimer biocompatibility and toxicity. *Adv. Drug Deliv. Rev*. **57**:2215–2237 (2005) doi:10.1016/j.addr.2005.09.019.
19. G. Domokos, B. Jopski, and K. H. Schmidt. Preparation, Properties and Biological Function of Liposome Encapsulated Hemoglobin. *Biomater. Artif. Cells Immobil. Biotechnol*. **20**:345–354 (1992).
20. G. S. Kwonand, and K. Kataoka. Block-Copolymer Micelles as Long-Circulating Drug Vehicles. *Adv. Drug Deliv. Rev*. **16**:295–309 (1995) doi:10.1016/0169-409X(95)00031-2.
21. J. A. Champion, Y. K. Katare, and S. Mitragotri. Particle shape: A new design parameter for micro- and nanoscale drug delivery carriers. *J. Control. Release*. **121**:3–9 (2007) doi:10.1016/j.jconrel.2007.03.022.
22. L. E. Euliss, J. A. DuPont, S. Gratton, and J. DeSimone. Imparting size, shape, and composition control of materials for nanomedicine. *Chem. Soc. Rev*. **35**:1095–1104 (2006) doi:10.1039/b600913c.
23. D. R. Arifinand, and A. F. Palmer. Stability of liposome encapsulated hemoglobin dispersions. *Artificial Cells Blood Substitutes and Biotechnology*. **33**:113–136 (2005) doi:10.1081/BIO-200055874.
24. S. L. Li, B. Byrne, J. Welsh, and A. F. Palmer. Self-assembled poly(butadiene)-b-poly(ethylene oxide) polymersomes as paclitaxel carriers. *Biotechnol. Prog*. **23**:278–285 (2007) doi:10.1021/bp060208+.
25. S. E. A. Gratton, P. D. Pohlhaus, J. Lee, J. Guo, M. J. Cho, and J. M. DeSimone. Nanofabricated particles for engineered drug therapies: A preliminary biodistribution study of PRINT (TM) nanoparticles. *J. Control. Release*. **121**:10–18 (2007) doi:10.1016/j.jconrel.2007.05.027.
26. J. P. Rolland, B. W. Maynor, L. E. Euliss, A. E. Exner, G. M. Denison, and J. M. DeSimone. Direct fabrication and harvesting of monodisperse, shape-specific nanobiomaterials. *J. Am. Chem. Soc*. **127**:10096–10100 (2005) doi:10.1021/ja051977c.
27. A. Fattorossi, R. Nisini, J. G. Pizzolo, and R. Damelio. New, Simple Flow-Cytometry Technique to Discriminate between Internalized and Membrane-Bound Particles in Phagocytosis. *Cytometry*. **10**:320–325 (1989) doi:10.1002/cyto.990100311.
28. R. M. Martin, H. Leonhardt, and M. C. Cardoso. DNA labeling in living cells. *Cytometry Part A*. **67A**:45–52 (2005) doi:10.1002/cyto.a.20172.
29. B. L. Clarkeand, and P. H. Weigel. Recycling of the Asialoglycoprotein Receptor in Isolated Rat Hepatocytes - Atp Depletion Blocks Receptor Recycling but Not a Single Round of Endocytosis. *J. Biol. Chem*. **260**:128–133 (1985).
30. E. Macia, M. Ehrlich, R. Massol, E. Boucrot, C. Brunner, and T. Kirchhausen. Dynasore, a cell-permeable inhibitor of dynamin. *Developmental Cell*. **10**:839–850 (2006) doi:10.1016/j.devcel.2006.04.002.
31. O. Harush-Frenkel, N. Debotton, S. Benita, and Y. Altschuler. Targeting of nanoparticles to the clathrin-mediated endocytic pathway. *Biochem. Biophys. Res. Commun*. **353**:26–32 (2007) doi:10.1016/j.bbrc.2006.11.135.
32. M. C. Garnett. Gene-delivery systems using cationic polymers. *Crit. Rev. Ther. Drug Carr. Syst*. **16**:147–207 (1999).
33. W. Zauner, M. Ogris, and E. Wagner. Polylysine-based transfection systems utilizing receptor-mediated delivery. *Adv. Drug Deliv. Rev*. **30**:97–113 (1998) doi:10.1016/S0169-409X(97)00110-5.